

## Supplementary Information

### **An axis-specific rotational rainbow in the direct scatter of formaldehyde from Au(111) and its influence on trapping probability**

G. Barratt Park,<sup>1,2, a)</sup> Bastian C. Krüger,<sup>1</sup> Sven Meyer,<sup>1</sup> Alexander Kandratsenka,<sup>2</sup> Alec M. Wodtke,<sup>1,2</sup> and Tim Schäfer<sup>1</sup>

<sup>1)</sup> *University of Goettingen, Institute for Physical Chemistry, Tammannstr. 6, 37077 Goettingen, Germany*

<sup>2)</sup> *Max Planck Institute for Biophysical Chemistry, Göttingen, Am Fassberg 11, 37077 Goettingen, Germany*

---

<sup>a)</sup> Electronic mail: barratt.park@mpibpc.mpg.de

## S.I. BACKING GAS MIXTURES

Table S.I lists the backing gas compositions used in this study to achieve incident kinetic energies of 0.11–1.21 eV. Also listed are the backing pressures and, where applicable, the measured rotational temperatures in the incident beam. Because interconversion of the ortho (odd  $K_a''$ ) and para (even  $K_a''$ ) species does not occur on the timescale of our experiment,<sup>1</sup> the two species are present in the incoming beam with the room temperature ortho:para ratio of 3:1, and we use the term “rotational temperature” to describe the state distribution within each manifold, considered as separate species.

TABLE S.I. Properties of the incoming molecular beam of formaldehyde, obtained with a range of backing gas mixtures and stagnation pressures. Incidence translational energy ( $E_i$ ) had no measurable dependence on the stagnation pressure,  $P_{\text{stag}}$ . Numbers in parentheses represent the  $1\sigma$  standard deviation of the final digit of the incidence energy, obtained from repeated measurements. Measured rotational temperatures are reliable to within  $\sim 15\%$ .

Backing Mixture	$E_i/\text{eV}$	$P_{\text{stag}}/\text{bar}$	$T_{\text{rot}}/\text{K}$
pure N <sub>2</sub>	0.11(2)	4	6
25% N <sub>2</sub> in H <sub>2</sub>	0.33(4)	12	
15% N <sub>2</sub> in H <sub>2</sub>	0.39(2)	12	
10% N <sub>2</sub> in H <sub>2</sub>	0.48(6)	10	
pure He	0.47(1)	3	15
		10.8	3
50% He in H <sub>2</sub>	0.88(9)	3	
		12	
pure H <sub>2</sub>	1.21(6)	6	8
		12	9

## S.II. METHOD FOR FITTING THE SPECTRA

The lines in the  $b$ -type  $\tilde{A} \leftarrow \tilde{X} 4_0^1$  spectra of rotationally hot scattering products are sufficiently dense that few individual rotational lines are fully resolved. Nevertheless, the spectra

contain sharp features that convey rich information about the rotational distribution in the scattering products, via the high quality spectroscopic Hamiltonians<sup>2,3</sup> that are available for this transition. This allows us to perform fits of the intensity profile both to a Boltzmann distribution and to a rotational rainbow model (see Section III of the main paper). Our experimentally observed lines are broadened at the baseline as a result of the spectral profile of the dye laser used to excite the  $\tilde{A} \leftarrow \tilde{X}$  transition. We obtain the lineshape function used in our fits by analyzing the fully resolved lineshape observed in the rotationally cold incoming molecular beam. For numerical simplicity, we fit the lineshape,  $I(f)$ , to the sum of a Lorentzian and a Gaussian component:

$$I(f) = A_L \frac{\Gamma^2}{(f - f_0)^2 + \Gamma^2} + A_G e^{-(f-f_0)^2/\sigma^2}, \quad (\text{S.1})$$

where  $f_0$  is the transition frequency,  $A_L$  and  $A_G$  characterize the relative contribution of the Lorentzian and Gaussian components, and  $\Gamma$  and  $\sigma$  characterize the Lorentzian and Gaussian widths, respectively. In all fits reported in this work, we used a line function with the parameters  $\Gamma = 0.1 \text{ cm}^{-1}$ ,  $\sigma = 0.4 \text{ cm}^{-1}$ ,  $A_L = 0.3$ , and  $A_G = 0.7$ . In cases where the dye laser power varied by more than 15% over the course of the scan, the spectral intensities were corrected by dividing by the measured laser power profile prior to fitting. Fitting was performed using a quasi-Newton algorithm.

### S.III. TRAPPING/DESORPTION CHANNEL: $T_s$ DEPENDENCE OF THE ROTATIONAL DISTRIBUTION

At the lowest incident kinetic energy employed in our study ( $E_i = 0.11 \text{ eV}$ ), the trapping/desorption mechanism dominates at the  $18^\circ$  scattering angle that was probed.<sup>4</sup> As a test for equilibration of rotational degrees of freedom to the surface, we have acquired REMPI spectra of molecules scattered in this regime. Figure S.I shows the  $\tilde{A} \leftarrow \tilde{X}$  ( $4_0^1$ ) REMPI spectra, acquired from molecules scattered at an incidence energy of  $E_i = 0.11 \text{ eV}$ , at various surface temperatures. Although we encountered difficulties from low signal-to-noise ratio in this regime—particularly at the lowest surface temperatures—the spectra display a clear dependence on surface temperature. Shown for comparison are the simulated absorption spectra with  $T_{\text{rot}} = T_s$ .

The rotationally resolved band structure of an asymmetric top molecule has a complicated appearance. However, there are several readily identifiable features in the type-*b* spectra

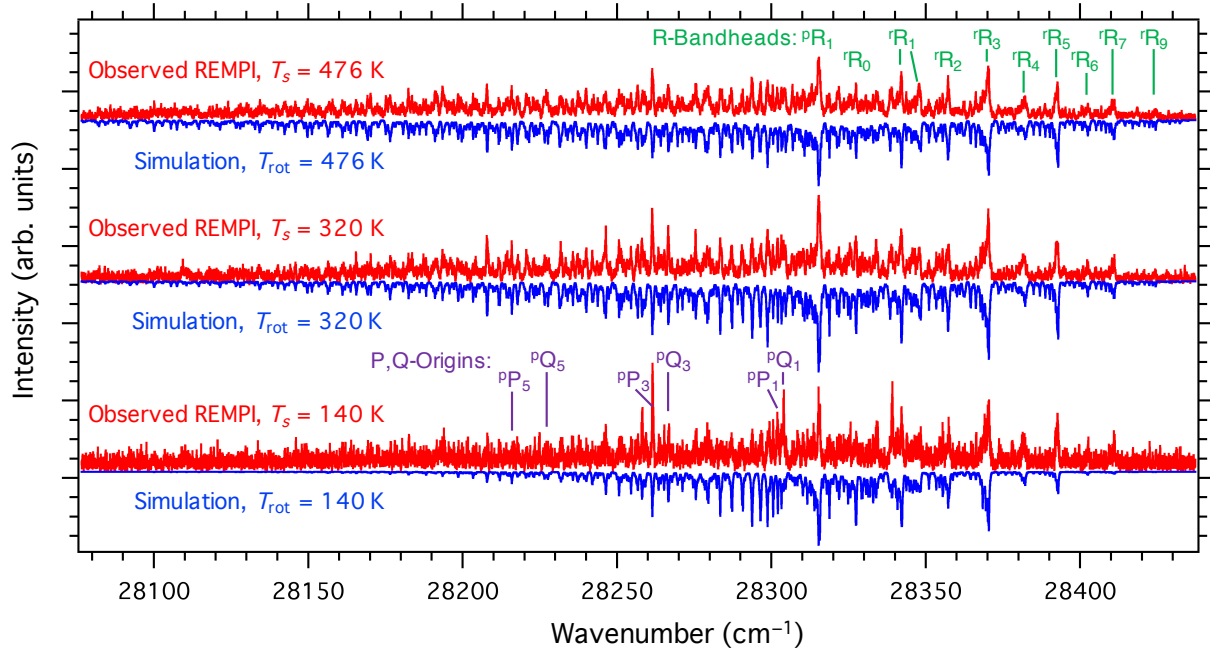


FIG. S.I. The  $1+1'$  REMPI spectrum of the  $\tilde{A} \leftarrow \tilde{X} (4_0^1)$  band of formaldehyde molecules, scattered from a Au(111) surface at  $E_i = 0.11$  eV, is shown as a function of surface temperature (red, upward directed peaks). Shown for comparison are the simulated spectra at  $T_{\text{rot}} = T_s$  (blue, downward directed peaks). The locations of selected R-bandheads and P- and Q-origins are labeled.

shown in Fig. S.I. First, at the high-frequency end of the band, there is a regularly-spaced progression of bandheads for the  ${}^rR_{K_a''}$  branches, which are labeled in the upper right corner of the figure. Each  ${}^rR_{K_a''}$  branch exhibits a bandhead at  $J'' \approx 7$ , and the 3:1 ortho:para intensity alternation between bandheads with odd and even  $K_a''$  is evident. (The  ${}^rR_1$  branch exhibits two bandheads because the asymmetry splitting in the  $K_a = 1$  manifold between  $e/f$  levels is well resolved.) As the temperature is increased, intensity grows in at higher values of  $K_a''$ , but the relative intensity at the bandheads decreases due to increased intensity from the higher- $J$  progression to the red of each bandhead.

Labeled in the bottom-center of Fig. S.I are the origins of several of the lowest  ${}^pQ$  and  ${}^pP$  branches, each of which exhibit progressions in  $J''$  that extend to the red. At low rotational temperature, these origins give rise to intense features in the spectrum, because of high population in low- $J''$  states. However, as the rotational temperature increases, these features lose intensity relative to the higher- $J''$  lines that gain intensity further to the red in the  ${}^pQ$ - and  ${}^pP$ -branch region. Note that at  $T_s = 140$  K (bottom of Fig. S.I), the  ${}^pQ_1$  feature

TABLE S.II. Fitted Boltzmann rotational temperature obtained from the  $\tilde{A} \leftarrow \tilde{X} (4_0^1)$  REMPI spectrum for formaldehyde molecules scattered in the trapping/desorption channel at  $E_i = 0.11 \pm 0.02$  eV from Au(111) two surface temperatures. Stated uncertainties in the fitted  $T_{\text{rot}}$  are  $1\sigma$ .

$T_s/\text{K}$	$T_{\text{rot}}/\text{K}$ (fit)
$320 \pm 15$	$338 \pm 32$
$476 \pm 1$	$498 \pm 48$

at  $28\,305\text{ cm}^{-1}$  is relatively intense, but at  $T_s = 476\text{ K}$  (top spectrum of Fig. S.I) the relative intensity of the feature disappears to a considerable extent. Finally, as the temperature increases, there is a general shift of band intensity to lower frequency, where the highest- $J$  transitions occur.

At the lowest surface temperature (140 K, bottom of Fig. S.I), we encountered problems with low signal-to-noise ratio. Although there are a few discrepancies between the spectrum and simulation, it is not possible to conclude whether the scattered molecules exhibit a significant departure from a Boltzmann distribution at  $T_{\text{rot}} = T_s$ . The upper two spectra in Fig. S.I (at 320 and 476 K) had sufficient signal-to-noise ratio to enable a reliable fit of the spectrum to a simulated spectrum obtained with a Boltzmann rotational distribution. The value of  $T_{\text{rot}}$  obtained from the fit (see Table S.II) agrees with  $T_s$ , to within the  $\sim 10\%$  uncertainty of the fit.

#### S.IV. TABULATION OF FIT PARAMETERS FOR THE DIRECT SCATTER ROTATIONAL DISTRIBUTIONS

The best-fit parameters to Eq. 1 for formaldehyde molecules directly scattered from the Au(111) surface over the range  $E_i = 0.33\text{--}1.21$  eV are tabulated in Table S.III. These parameters are plotted in Fig. 4, and the corresponding best-fit spectra are shown in Figs. 1–3. Also tabulated is the percent improvement in the root mean square error (RMSE) that is obtained from the fit to Eq. 1, relative to the RMSE obtained from a fit to a Boltzmann distribution.

TABLE S.III. Best-fit parameters obtained by fitting the spectra of scattered molecules to Eq. 1, with the constraints  $T_{bc} = T_a = T$  and  $\sigma_a = 850 \text{ cm}^{-1}$ . The spectrum was acquired several times at each  $E_i$  and the values tabulated are the average and  $1\sigma$  standard deviation of the values obtained from repeated fits. The final column tabulates the average percent improvement,  $R_i$ , in the root mean square error of the fit,  $R_{\text{fit}}$ , relative to the RMSE obtained from a fit to a Boltzmann temperature,  $R_b$ .  $R_i = (1 - R_b/R_{\text{fit}}) \times 100\%$ .

$E_i/\text{eV}$	$T/\text{K}$	$S$	$E_0/\text{cm}^{-1}$	$R_i/\%$
1.21	$820 \pm 120$	$0.58 \pm 0.26$	$970 \pm 80$	18.0
0.88	$910 \pm 290$	$0.47 \pm 0.05$	$870 \pm 80$	11.4
0.48	$690 \pm 140$	$0.27 \pm 0.10$	$720 \pm 60$	5.3
0.47	$790 \pm 150$	$0.32 \pm 0.17$	$880 \pm 70$	8.8
0.39	$770 \pm 150$	$0.26 \pm 0.09$	$480 \pm 80$	1.8
0.33	$570 \pm 90$	$0.14 \pm 0.18$	$460 \pm 50$	0.5

## S.V. ROTATIONAL STATE DEPENDENCE OF SCATTERED BEAM VELOCITY

Due to experimental considerations, it is challenging for us to make precise rotationally resolved time-of-flight measurements. There are two principal limitations. First, since we do not have a tagging scheme available to us, we measure the arrival time distribution that results from the full incoming molecular beam profile, which is approximately Gaussian in shape with a typical width of  $\sim 30 \mu\text{s}$  (FWHM). Second, due to the experimental design of the 157 nm VUV beam propagation, we are able to vary the REMPI probe position by only 6 mm, resulting in low time-of-flight resolution. However, we are able to make crude rotationally resolved speed measurements for a representative selection of rotational states, which allows us to evaluate the extent to which the neglect of density-to-flux conversion affects our estimation of relative rotational state populations.

A beam of formaldehyde seeded in  $\text{H}_2$  ( $E_i = 1.21 \text{ eV}$ ) was scattered from the Au(111) surface and the  $1 + 1'$  REMPI signal was probed at distances 4–10 mm from the surface. The arrival time distribution was measured by scanning the delay between the pulsed nozzle and the probe lasers. The directly scattered beam profile resembles that of the incoming

TABLE S.IV. The rotationally-resolved average final kinetic energy,  $\langle E_f \rangle$ , that results from direct scatter at  $E_i = 1.21$  eV. The total rotational energy ( $E''_{\text{rot}}$ ) and the projection of rotational energy about the  $a$ -axis ( $E''_a$ ) of the lower state of each probe transition is also tabulated. The uncertainty is obtained from the standard error of the fit to the velocities shown in Fig. S.II.

Transition	Wavenumber/cm <sup>-1</sup>	$E''_{\text{rot}}$ /eV	$E''_a$ /eV	$\langle E_f \rangle$
<sup>r</sup> PQ <sub>1,8</sub> (9)	28 318.80	0.015	0.0012	0.58 ± 0.17
<sup>r</sup> R <sub>5</sub> (5–8)	28 392.80	0.030–0.036	0.0292	0.49 ± 0.11
<sup>r</sup> R <sub>13</sub> (13)	28 434.77	0.197	0.1967	0.44 ± 0.15

beam, which implies that broadening due to the distribution of scattering velocity is small relative to the distribution of time at which molecules in the incoming beam impinge upon the surface. The mean arrival time at each probe position is therefore estimated by fitting the arrival distribution to a Gaussian. Measurements performed at different incident kinetic energies have shown that the dependence of  $\langle E_f \rangle$  on  $\langle E_i \rangle$  in the direct scattering channel follows near Baule limit behavior for scattering from a hard sphere with the mass of a single gold atom.<sup>4</sup>

The measurement was repeated at three different REMPI frequencies. We probed the well resolved features arising from <sup>r</sup>R<sub>13</sub>(13) and <sup>r</sup>Q<sub>1</sub>(9) as well as the incompletely resolved <sup>r</sup>R<sub>5</sub>(5–8) bandhead. The results are summarized in Table S.IV and the mean arrival time data is plotted in Fig. S.II. The 7% deviation in the three measured speeds is less than the ~14% uncertainty in the speed determination and is therefore not statistically significant. Within the range  $E_{\text{rot}} = 0$ –0.2 eV, the variation in  $\langle E_f \rangle$  with the scattered rotational state is probably smaller than this. We conclude that the upper limit of  $\Delta v / \langle v \rangle$  for direct scattering into different rotational levels at  $E_i = 1.21$  eV is on the order of 10%. This means that errors due to the neglect of the rotational state dependent density-to-flux conversion are much too small to give rise to the observed non-Boltzmann relative intensities.

## REFERENCES

<sup>1</sup>R. F. Curl, Jerome V. V. Kasper, and Kenneth S. Pitzer. Nuclear spin state equilibration through nonmagnetic collisions. *The Journal of Chemical Physics*, 46(8):3220–3228, 1967.

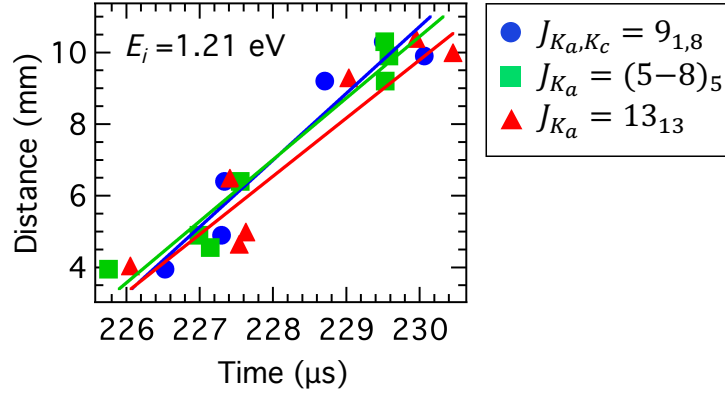


FIG. S.II. Rotationally resolved mean arrival time (relative to the pulsed nozzle trigger) of formaldehyde molecules directly scattered from a Au(111) surface, probed at different distances from the surface. Rotational quantum numbers of the probed states are given in the legend. The slopes of the trend lines correspond to mean scattering velocities of  $1870 \pm 280$ ,  $1720 \pm 190$ , and  $1640 \pm 270$  m/s for the  $9_{1,8}$ ,  $(5-8)_5$ , and  $13_{13}$  states, respectively.

<sup>2</sup>D. J. Clouthier and D. A. Ramsay. The spectroscopy of formaldehyde and thioformaldehyde. *Annual Review of Physical Chemistry*, 34:31–58, 1983.

<sup>3</sup>H. S. P. Müller, G. Winnewisser, J. Demaison, A. Perrin, and A. Valentin. The ground state spectroscopic constants of formaldehyde. *Journal of Molecular Spectroscopy*, 200(1):143–144, 2000.

<sup>4</sup>Bastian C. Krüger, G. Barratt Park, Sven Meyer, Roman J. V. Wagner, Alec M. Wodtke, and Tim Schäfer. Trapping-desorption and direct-scattering of formaldehyde at Au(111). *In preparation*, 2017.